A Cohesive-Frictional Interface Model with Frictional Properties Degradation

G. Borino, B. Failla, F. Parrinello
Università di Palermo, Dipartimento di Ingegneria Strutturale e Geotecnica – DISeG, Palermo, Italy

1. Introduction

Mechanical interface are widely employed in order to model fracture propagation phenomena along pre-assigned surfaces [1-8]. Several aspects are involved in the description of the interface behavior. This paper is devoted to present an interface constitutive modeling which couples a cohesive behavior, based on the damage mechanics theory, with a frictional one, defined in a non-associative plasticity framework. By means of a specific interpretation of the damage variable, the formulation follows the transition of the initial sound interface material, up to the fully cracked condition [9,10]. The macrocrack surface has initial frictional properties and is subjected to degradation phenomena. Namely, the smoothing and breaking of surface asperities causes a progressive reduction of dilatancy effects and of the frictional angle. These phenomena are modeled as uncoupled: dilatancy saturation is assumed to occur when relevant internal variable reach a limit value; frictional strength reduction occurs as effect of oligocyclic process, which takes place during the plastic sliding between the macrocrack surfaces.
The constitutive framework presented in this paper belongs to the class of interface damage models. The frictional phenomena that develops in sliding deformation modes, in case of closure of the damaged interface, are modeled by nonassociative plasticity laws. The model is developed in a fully compliance with thermodynamic principles. Finite element numerical tests are presented in order to show the main features of the proposed model.

2. Formulation

It is recognized that damage internal variable, ω, can be geometrically associated to some cracked fraction of a reference surface, namely

$$\omega = \frac{dS_c}{dS} \equiv \frac{dS - dS_s}{dS}, \tag{1}$$

where dS_c and dS_s are respectively the cracked and sound parts of the reference surface dS at a generic point of the interface (see Fig. 1). By the definition given in Eq. (1) damage variable ranges in between $0 \le \omega \le 1$, where $\omega = 0$ means initial sound state ($dS_c = 0, \quad dS_s = dS$), whereas $\omega = 1$ means fully cracked state ($dS_s = 0, \quad dS_c = dS$). Adopting a mixture approach, induced by the fact that damage allows to define at each interface point two fractions, it is possible to derive the overall constitutive relation as a result of assigning a simple

constitutive law for each fraction. The interface constitutive relations are then derived enforcing at a microscale relevant congruence and equilibrium relations, that as pointed out by Alfano and Sacco [9], allows to consider the proposed approach as a multiscale approach, in which the overall interface constitutive relation are derived looking at a subscale (the two fractions) micro-model.

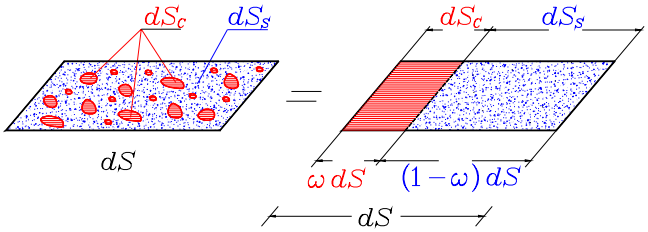

Figure.1 Sketch of the damaged interface and the equivalent two fraction model.

Since interface models are adopted to drive decohesion processes along a prefixed surface, the kinematic variable that describe the deformation induced at a point of the interface is the displacement discontinuity vector $[\![\boldsymbol{u}]\!]$, defined as $[\![\boldsymbol{u}]\!] = \boldsymbol{u}^+ + \boldsymbol{u}^-$, where $\boldsymbol{u}^+$ and $\boldsymbol{u}^-$ are the displacement vectors valuated at the upper and lower part of the interface. Since the proposed model is identified by two fractions, it is possible to adopt a specific kinematic rule able to describe the material state of each fraction. In the following the indices *s* and *c* are adopted to define the sound and the micro-cracked fraction respectively. The overall internal congruence requires that the (external) strain is the same for both (internal) fractions

$$[\![\boldsymbol{u}_c]\!] = [\![\boldsymbol{u}_s]\!] = [\![\boldsymbol{u}]\!]. \tag{2}$$

As far as the material state for each fraction is concerned the following kinematic rules are adopted:

– *Sound fraction*. Neither plastic nor damage deformation can develop at the sound fraction. It follows that deformation is only elastic

$$[\![\boldsymbol{u}]\!] = [\![\boldsymbol{u}_s]\!] = \boldsymbol{\delta}_s^e \,. \tag{3}$$

– *Micro-cracked fraction*. The total deformation is given as the sum of several contributions, namely

$$[\![\boldsymbol{u}]\!] = [\![\boldsymbol{u}_c]\!] = \boldsymbol{\delta}_c^e + \boldsymbol{\delta}_c^p + \boldsymbol{\delta}_c^d \,, \tag{4}$$

Where $\boldsymbol{\delta}_c^e$ is the elastic component, $\boldsymbol{\delta}_c^p$ is the plastic, or frictional, component and $\boldsymbol{\delta}_c^d$ is the damage, or detachment component. A physical meaning to these deformation variables is shown in Fig. 2, where starting from the micro-cracked undeformed state (Fig. 2a), it can be observed that the deformation $\boldsymbol{\delta}_c^e$ is associated to some elastic behaviour induced by reversible deformations of the micro-asperities produced by the formations of the micro-cracks when they are in

a contact state (Fig. 2b). The vector $\boldsymbol{\delta}_c^p$ is related to the irreversible sliding (including normal dilatancy), and it is active when a frictional yield strength is attained (Fig. 2c). Frictional or plastic components may develop only under normal compressive state. On the contrary, no positive normal traction (tensile) can be sustained in the micro-cracked fraction, since in this case no more contact between micro-cracked edges is possible and a opening displacement vector $\boldsymbol{\delta}_c^d$ is then produced (Fig. 2d)

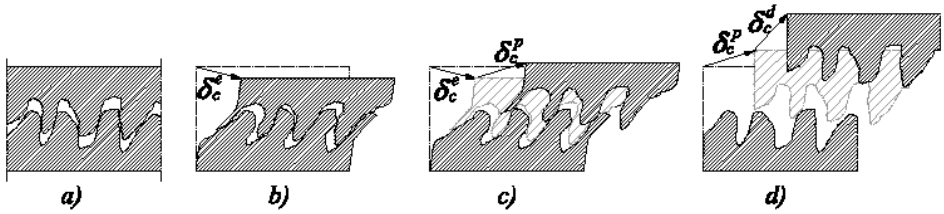

Figure.2 Sketch of the kinematic deformation modes at the micro-cracked fraction.

The unilateral contact and the related frictional deformation are characterized by the condition that the displacement jump normal component (denoted by the index *N*) must have a nonpositive elastic component δ_{cN}^e and a nonnegative detachment component δ_{cN}^d. Moreover, due to the evidence that elastic deformation $\boldsymbol{\delta}_c^e$ and normal component, δ_{cN}^d, cannot be both different from zero at the same time, the following complementarity condition holds

$$\delta_{cN}^e \le 0, \qquad \delta_{cN}^d \ge 0, \qquad \delta_{cN}^e \, \delta_{cN}^d = 0 . \tag{5}$$

The tangential component (denoted by the index *T*) of the elastic deformation vector, δ_{cT}^e has no sign restriction, but it is also subjected to the complementarity condition

$$\delta_{cT}^e \, \delta_{cN}^d = 0 . \tag{6}$$

No constraint exists for the tangential component of the detachment vector, δ_{cT}^d, which means that for re-closing conditions, residual tangential components may be present $(\delta_{cT}^d \neq 0)$. Relations (5) and (6) are also true written in rate form.

3. Thermodynamic constitutive framework

The interface material state can be represented by the Helmholtz free energy density (for unit surface) and, since the proposed approach is based on the superposition of two fractions, the following expression is adopted

$$\begin{aligned} \psi(\boldsymbol{\delta}_s^e, \boldsymbol{\delta}_c^e, \omega, \xi, \xi_{fr}, \xi_{dl}) = (1-\omega)\, \bar{\psi}_s^e(\boldsymbol{\delta}_s^e) + \omega\, \bar{\psi}_c^e(\boldsymbol{\delta}_c^e) + \psi_d^{in}(\xi) \\ + \psi_{fr}^{in}(\xi_{fr}) + \psi_{dl}^{in}(\xi_{dl}). \end{aligned} \tag{7}$$

where $\bar{\psi}_s^e$ and $\bar{\psi}_c^e$ are the elastic free energy densities related to the sound and micro-cracked fractions respectively, ψ_d^{in} is the internal free energy related to the internal damage hardening, function of the scalar internal variable ξ. Finally, the

two internal state free energy densities ψ_{fr}^{in} and ψ_{dl}^{in} are introduced in order to describe two material state evolution. ψ_{fr}^{in} is related to the fact that the frictional coefficient evolves from an initial value to a smaller final one. ψ_{dl}^{in} is related to the observed evidence that frictional dilatancy tends to saturate as deformation develops. The two internal state phenomena, even if physically different, can be modeled in the same manner, namely a transition (or saturation) function can be invoked. Namely, as deformation develops, the frictional parameter and the dilatancy coefficient evolves. The first decrease up to a constant final value, the second decrease up to zero. The specific choice of ψ_{fr}^{in} and ψ_{dl}^{in} is not unique and in the Sect. 3.4 a simple choice is proposed.
The elastic fractions of the free energy, for linear elasticity, are quadratic forms

$$\bar{\psi}_s^e(\boldsymbol{\delta}_s^e) = \frac{1}{2}\boldsymbol{\delta}_s^{eT}\mathbf{K}^s\boldsymbol{\delta}_s^e; \qquad \bar{\psi}_c^e(\boldsymbol{\delta}_c^e) = \frac{1}{2}\boldsymbol{\delta}_c^{eT}\mathbf{K}^c\boldsymbol{\delta}_c^e \tag{8a,b}$$

Representing the stored strain energy at the two fractions each of which, in accord to Eq. (7), has the weight coefficient $(1-\omega)$ and ω, respectively. $\mathbf{K}^s$ and $\mathbf{K}^c$ are diagonal matrices collecting the elastic moduli K_i^s, K_i^c for the sound and micro-cracked fraction, respectively (i=N, T for the two Cartesian components).
Thermodynamic consistency requires the satisfaction of the Clausius-Duhem inequality, which in turn is able to define the intrinsic dissipation

$$D = \boldsymbol{t}^T[\![\dot{\boldsymbol{u}}]\!] - \dot{\psi} \geq 0\,. \tag{9}$$

Expanding Eq. (7) and taking Eqs. (3), (4) in rate form $\dot{\boldsymbol{\delta}}_s^e = [\![\dot{\boldsymbol{u}}]\!]$, $\dot{\boldsymbol{\delta}}_c^e = [\![\dot{\boldsymbol{u}}]\!] - \dot{\boldsymbol{\delta}}_c^p - \dot{\boldsymbol{\delta}}_c^d$, dissipation is expressed as

$$\begin{aligned} D = &\left(\boldsymbol{t} - \frac{\partial\psi}{\partial\boldsymbol{\delta}_s^e} - \frac{\partial\psi}{\partial\boldsymbol{\delta}_c^e}\right)^T [\![\dot{\boldsymbol{u}}]\!] + \left(\frac{\partial\psi}{\partial\boldsymbol{\delta}_c^e}\right)^T \left(\dot{\boldsymbol{\delta}}_c^p + \dot{\boldsymbol{\delta}}_c^d\right) - \frac{\partial\psi}{\partial\omega}\dot{\omega} - \frac{\partial\psi_d^{in}}{\partial\xi}\dot{\xi} \\ &- \frac{\partial\psi_{fr}^{in}}{\partial\xi_{fr}}\dot{\xi}_{fr} - \frac{\partial\psi_{dl}^{in}}{\partial\xi_{dl}}\dot{\xi}_{dl} \geq 0. \end{aligned} \tag{10}$$

In case of purely elastic loading, $\dot{\omega} = \dot{\xi} = \dot{\xi}_{fr} = \dot{\xi}_{dl} = 0$, $\dot{\boldsymbol{\delta}}_c^p = \dot{\boldsymbol{\delta}}_c^d = \mathbf{0}$, no dissipation is produced for any reversible deformation mechanism $[\![\dot{\boldsymbol{u}}]\!]$, then the first term of Eq. (10) gives the interface elastic constitutive relations

$$\boldsymbol{t} = \frac{\partial\psi}{\partial\boldsymbol{\delta}_s^e} + \frac{\partial\psi}{\partial\boldsymbol{\delta}_c^e} := \boldsymbol{t}_s + \boldsymbol{t}_c \tag{11}$$

where

$$\boldsymbol{t}_s := \frac{\partial\psi}{\partial\boldsymbol{\delta}_s^e} = (1-\omega)\mathbf{K}_s\boldsymbol{\delta}_s^e, \qquad \boldsymbol{t}_c := \frac{\partial\psi}{\partial\boldsymbol{\delta}_c^e} = \omega\,\mathbf{K}_c\boldsymbol{\delta}_c^e, \tag{12a,b}$$

in which $\boldsymbol{t}_s$ and $\boldsymbol{t}_c$ play the role of internal traction vectors acting at each fraction and a micro-scale balance requires $\boldsymbol{t} = \boldsymbol{t}_s + \boldsymbol{t}_c$ (See Fig. 3). Moreover, as a consequence of the unilateral constraints of Eqs. (6) and (7), it follows

$$t_{cN} \le 0, \qquad \text{always} \tag{13a}$$

$$t_{cT} \ne 0, \qquad \text{only if} \quad t_{cN} < 0. \tag{13b}$$

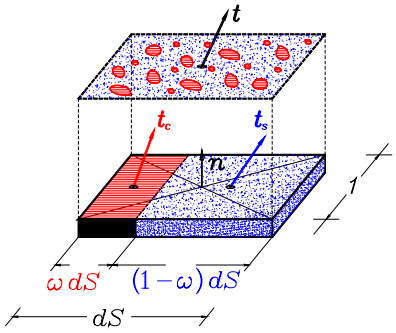

Figure.3 Interface static variables, $\boldsymbol{t}_s$ and $\boldsymbol{t}_c$ at the two fractions and the overall traction vector $\boldsymbol{t}$.

Following a classical thermodynamic reasoning path, state equations (12) holds for any dissipative deformation processes, so that for a very general dissipative deformation, Eq. (10) takes the form

$$D = Y\dot{\omega} + \boldsymbol{t}_c^T\left(\dot{\boldsymbol{\delta}}_c^p + \dot{\boldsymbol{\delta}}_c^d\right) - \chi\dot{\xi} - \chi_{fr}\dot{\xi}_{fr} - \chi_{dl}\dot{\xi}_{dl} \ge 0, \tag{14}$$

where the following definitions of energy conjugated forces have been assumed

$$Y := \frac{\partial\psi}{\partial\omega} = \frac{1}{2}[\![\boldsymbol{u}]\!]^T\,\mathbf{K}_s\,[\![\boldsymbol{u}]\!] - \frac{1}{2}\boldsymbol{\delta}_c^{eT}\mathbf{K}_c\boldsymbol{\delta}_c^e, \tag{15}$$

$$\chi := \frac{\partial\psi_d^{in}}{\partial\xi}, \tag{16}$$

$$\chi_{fr} := \frac{\partial\psi_{fr}^{in}}{\partial\xi_{fr}}, \qquad \chi_{dl} := \frac{\partial\psi_{dl}^{in}}{\partial\xi_{dl}}. \tag{17a,b}$$

Equation (15) gives the expression of the energy release rate; namely, the energy dissipated for a unit damage increment. At difference with the usual formulations, the classical first term related to $[\![\boldsymbol{u}]\!]$, needs to be subtracted by a second term describing the strain energy trapped at the microscale elastic deformation ($\boldsymbol{\delta}_c^e$). The latter energy, related to the elastic deformation of the asperities, is not available to drive damage production.

Internal variable χ is the thermodynamic conjugated force to ξ and then is devoted to describe damage hardening state. The specific choice of the functional and its specific features are discussed in Sect. 3.3. Finally, the variables χ_{fr} and χ_{dl} are the thermodynamic conjugated forces to ξ_{fr} and ξ_{dl}. Their function is to describe changes in the frictional and dilatancy states. A discussion on a specific choice of Eq. (17) and the related potentials ψ_{fr}^{in} and ψ_{dl}^{in} is presented in Sect. 3.4.

Considering unilateral constraints given by Eqs. (6) and (7), written in rate form, together with the constraints of Eqs. (13), it follows that there cannot be an increment of the gap displacement $\dot{\boldsymbol{\delta}}_c^d$ in a contact state $\boldsymbol{t}_c \neq \mathbf{0}$, it then follows the orthogonality condition $\boldsymbol{t}_c^T \dot{\boldsymbol{\delta}}_c^d = 0$, which allows to write the dissipation in the following essential form

$$D = Y\dot{\omega} + \boldsymbol{t}_c^T \dot{\boldsymbol{\delta}}_c^p - \chi\dot{\xi} - \chi_{fr}\dot{\xi}_{fr} - \chi_{dl}\dot{\xi}_{dl} \geq 0\,. \tag{18}$$

It can be observed that the dissipation of Eq. (18) has a damage-frictional uncoupled structure. Namely, no dissipative interaction exists between the two phenomena. This means that an increment of damage (decohesion growth) does not involve a change in the frictional state and, at the same time, frictional deformation modes do not involve increment of damage. Separating the internal state variables, two dissipation functional can be recognized

$$D = D_d + D_p\,, \tag{19}$$

$$D_d(Y, \chi; \dot{\omega}, \dot{\xi}) = Y\dot{\omega} - \chi\dot{\xi} \geq 0; \tag{20a}$$

$$D_p(\boldsymbol{t}_c, \chi_{fr}, \chi_{dl}; \dot{\boldsymbol{\delta}}_c^p, \dot{\xi}_{fr}\dot{\xi}_{dl}) = \boldsymbol{t}_c^T \dot{\boldsymbol{\delta}}_c^p - \chi_{fr}\dot{\xi}_{fr} - \chi_{dl}\dot{\xi}_{dl} \geq 0, \tag{20b}$$

where D_d and D_p are the dissipation functionals related to damage (decohesion) and to frictional (plastic) mechanisms. The fact that dissipation splits in two contributes allows to introduce two distinct activation criteria, which independently govern formation and evolution of damage and friction.

3.1 Damage activation and flow rules

According to the structure, and to the static variables involved in the damage dissipation of Eq. (20a), interface damage is governed by an activation function in which the energy release rate, Y, is the driving force obeying to the inequality

$$\phi_d(Y, \chi) = Y - \chi - Y_0 \leq 0\,, \tag{21}$$

where Y_0 is the initial damage activation threshold, the variable χ describes the threshold increment evolution (damage hardening). For the initial virgin state $\chi = 0$, and then uniformly growths ($\dot{\chi} \geq 0$) with the damage flow laws below reported. This structure means that for a further damage production, the energy release rate must attain an higher threshold, defined as ($Y = \chi + Y_0$).
Assuming an associative structure, the related flow rules and the loading/unloading conditions reads

$$\dot{\omega} = \frac{\partial \phi_d}{\partial Y}\dot{\lambda}_d = \dot{\lambda}_d\,, \qquad \dot{\xi} = -\frac{\partial \phi_d}{\partial \chi}\dot{\lambda}_d = \dot{\lambda}_d\,, \tag{22a,b}$$

$$\dot{\lambda}_d \geq 0, \qquad \phi_d\dot{\lambda}_d = 0, \qquad \dot{\phi}_d\dot{\lambda}_d = 0 \tag{23}$$

It can be proved that to enforce positiveness of damage dissipation of Eq. (20a) the condition on the interface elastic moduli $K_N^s \geq K_N^s > 0$ and $K_T^s \geq K_T^s > 0$ must be satisfied. Moreover, since the internal variable $\chi > 0$ for $\xi = \lambda_d > 0$ and $\chi = 0$ only for $\xi = 0$, it follows that ψ_d^{in} must be convex for $\xi \geq 0$.

3.2 Frictional activation and flow rules

According to the structure and to the static variables involved in the frictional dissipation of Eq. (20b), frictional activation, at the micro-cracked fraction, is governed by a Mohr-Coulomb yield function

$$\phi_p(\boldsymbol{t}_c, \chi_{fr}) = (1 + a\ \chi_{fr})\left|t_{cT}\right| + \alpha_i\, t_{cN} \le 0 \tag{24}$$

where α_i is the initial frictional coefficient. As frictional deformation develops following the flow rules reported below, the frictional coefficient become

$$\alpha = \frac{\alpha_i}{1 + a\ \chi_{fr}}. \tag{25}$$

The frictional state law is posed in such a way (as it will be shown in Sec. 3.4) that the frictional internal variable is $0 \le \chi_{fr} \le 1$, with $\chi_{fr} = 0$ for the virgin state and $\chi_{fr} = 1$ as the frictional state reach a final constant condition. The final frictional coefficient is $\alpha_f = \alpha_i / (1 + a)$ which allows to derive the meaning and the value of the material constant $a = (\alpha_i - \alpha_f) / \alpha_f$.

At difference with damage, frictional does not possess an associative flow rule. In fact, it is well known that for a frictional material, associative rules would predict an excessive non-physical amount of plasticity dilatant deformation. Actually, what is observed is that dilatancy deformation is produced only at the very initial phase of plastic sliding. The initial dilatancy is often explained as due to the interlocking of the asperities which before breakings have to undergo a step over mechanism which produce the initial mesoscale dilatancy. A typical way adopted in the theory of plasticity to overcome this problem is to employ a non-associative approach in which the following plastic potential is defined

$$\Omega_p(\boldsymbol{t}_c, \chi_{fr}, \chi_{dl}) = (1 + a\ \chi_{fr})\left|t_{cT}\right| + \beta_i \left(1 - \chi_{dl}\right) t_{cN} \tag{26}$$

where β_i is the initial dilatancy coefficient (typically $\beta_i < \alpha_i$). Flow rules and loading/unloading conditions are then given as

$$\dot{\delta}^p_{cN} = \frac{\partial \Omega_p}{\partial\, t_{cN}} \dot{\lambda}_p = \beta_i \left(1 - \chi_{dl}\right) \dot{\lambda}_p, \quad \dot{\delta}^p_{cT} = \frac{\partial \Omega_p}{\partial\, t_{cT}} \dot{\lambda}_p = \operatorname{sgn}\left(t_{cT}\right)\left[1 + a\chi_{fr}\right] \dot{\lambda}_p, \tag{27a,b}$$

$$\dot{\xi}_{fr} = -\frac{\partial \Omega_p}{\partial\, \chi_{fr}} \dot{\lambda}_p = -a\left|t_{cT}\right| \dot{\lambda}_p, \qquad \dot{\xi}_{dl} = -\frac{\partial \Omega_p}{\partial\, \chi_{dl}} \dot{\lambda}_p = \beta_i\, t_{cN}\, \dot{\lambda}_p, \tag{28a,b}$$

$$\dot{\lambda}_p \ge 0, \qquad \phi_p \dot{\lambda}_p = 0, \qquad \dot{\phi}_p \dot{\lambda}_p = 0. \tag{29}$$

As done for the frictional internal variable χ_{fr}, if the state law for the dilatancy internal variable is such that $0 \le \chi_{dl} \le 1$, with $\chi_{dl} = 0$ for the virgin state and $\chi_{dl} = 1$, for the final stationary state. It can be observed by Eq. (26), that since dilatancy evolves with the law $\beta = \beta_i(1 - \chi_{dl})$, the stationary condition corresponds to a dilatancy saturation condition. Namely, the final value $\beta_f = 0$, and by Eq. (27a) no more plastic dilatancy deformation is produced $\dot{\delta}^p_{cN} = 0$.

3.3 Damage hardening law

The damage hardening, defined by the internal free energy ψ_d^{in}, can be assigned in different forms, depending on the specific shape of the softening normal traction – normal opening displacement law to be modeled. The most simple bi-linear case (see Fig. 4a) for a pure opening mode I ($t_T = 0$, $t_N > 0$) is obtained by the following definitions

$$\psi_d^{in}(\xi) = \frac{1}{2} K_N^s \bar{u}_e^2 \left[\frac{A^2}{A-\xi} - \xi \right]; \qquad \chi = \frac{\partial \psi_d^{in}}{\partial \xi} = \frac{1}{2} K_N^s \bar{u}_e^2 \left[\frac{A^2}{(A-\xi)^2} - 1 \right] \tag{30a,b}$$

where $A = \bar{u}_f / (\bar{u}_f - \bar{u}_e)$ in which $\bar{u}_e$ and $\bar{u}_f$ are the elastic limit and fully opened displacement jump for a simple opening deformation mode (see Fig.4a)

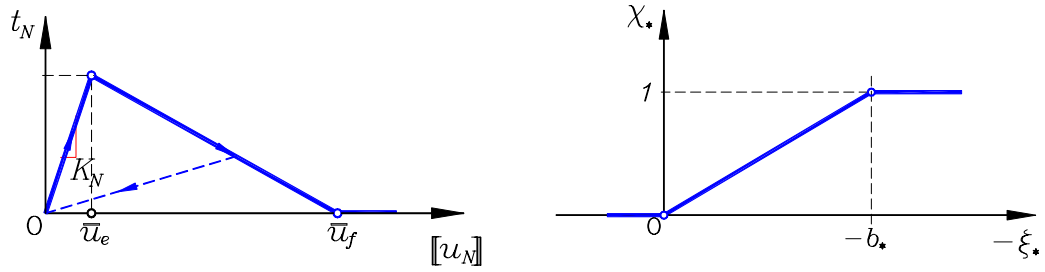

a) b)

Figure.4 a) bi-linear normal traction – opening displacement law. b) saturation function.

3.4 Frictional and dilatancy saturation functional

As pointed out in Secs. 3.1 and 3.2. the two internal variables χ_{fr} and χ_{dl} describe two different material phenomena, namely frictional coefficient evolution and evolution of the dilatancy parameter. Despite of their physical difference, they both describes a saturation phenomena, since the start from a zero value $\chi_* = 0$ (* being an index for *fr* or *dl* alternatively) for the virgin initial state, and evolving up to $\chi_* = 1$ as the relevant deformation process reach some assigned value b_*. The most simple choice of function of this kind is a linear transition law (see Fig. 4b) to which corresponds

$$\psi_*^{in}(\xi_*) = \frac{\langle -\xi_* \rangle^2}{2\, b_*} - \frac{\langle -\xi_* - b_* \rangle^2}{2\, b_*}; \qquad \chi_* = \frac{\partial \psi_*^{in}}{\partial \xi_*} = \frac{\langle -\xi_* \rangle}{b_*} - \frac{\langle -\xi_* - b_* \rangle}{b_*} \tag{31a,b}$$

Where the symbol $\langle x \rangle$ is a functional defined as $\langle x \rangle = (x + |x|)/2$.

It should be noted that both kinematic internal variables are intrinsically negative $\xi_{fr} < 0$ and $\xi_{dl} < 0$, as it emerges by the flow rules of Eqs. (28). In particular in Eq. (28a) a is a positive constant by its physical meaning discussed in Eq. (25), and in Eq. (28b) in order to activate frictional deformations it must be $t_{cN} \le 0$ (compressive state).

4. Numerical application

The constitutive model has been implemented in an open source finite element code by developing a specific six-nodes interface element. A simple example has been considered in order to qualitatively investigate the features of the constitutive model. The analyses regard a small portion of a brick-wall with length of 500 mm and height of 220 mm, shown in Fig. 5. Bricks are assumed elastic with Yung modulus E = 1800 MPa and Poisson ratio $\nu = 0.15$, whereas the mortar joints are modelled by the constitutive model above proposed, assuming the following parameters: sound and cracked fractions elastic stiffness $K_N^s = K_N^c$ = 1000 MPa/mm, $K_T^s = 900$ MPa/mm, K_T^c=200 MPa/mm, frictional and initial dilatancy angles are $\alpha_i = 30°, \beta_i = 20°$, maximum elastic and ultimate displacements are $\overline{u}_e = 3.0\,10^{-5}, \overline{u}_f = 2.0\,10^{-2}$, frictional and dilatancy saturation parameters are $a = 0.3, b_{fr} = 0.2, b_{dl} = 0.0015$.

The bottom and the top sections of the wall are connected, by mortar joints, to two rigid blocks whose displacements are constrained. In detail: the bottom rigid block is fixed, whereas the top rigid block is subjected to an imposed constant vertical displacement $u_y = -0.01\,\text{mm}$ and to a variable horizontal displacement. The analyses are performed for two different loading paths of the imposed horizontal displacement: a monotonic one and a cyclic one.

In order to understand the improvement provided by the strength reduction and by the dilatancy saturation, adopted in this paper, numerical simulations have been performed under three different constitutive hypothesis:

- Elastic Perfectly Plastic (EPP) behaviour of the frictional fraction;
- Elastic-Plastic (EP) with only dilatancy degradation;
- EP with both dilatancy degradation and resistance reduction.

The numerical results, obtained with the three specific constitutive assumption and performed with a monotonically increasing law of the imposed horizontal displacement, are compared in Figs. 6, respectively in terms of mean tangential (R_x /A) and normal stress (R_y /A) on the top and bottom sections *vs* horizontal displacement u_x. R_x and R_y are the overall reaction components and A the horizontal section area. Results of Fig. 6a show that the EPP model produces an unrealistic unlimited tangential strength; in fact, because of the dilatancy induced continuous development of normal plastic strain at the interface, an increasing compressive self-stress state is generated, which causes a proportional increment of the frictional tangential strength. As it can be observed in Fig. 6b, the mean normal stress at the constrained sections is constant in the elastic regime, whereas it monotonically increases when the frictional yield surface is attained. With reference to the EP behaviour with dilatancy degradation, numerical results, plotted in Fig. 6a, exhibit a residual frictional tangential strength, which remains constant for further horizontal displacement increments. Therefore, dilatancy

saturation prevents the tangential strength from unbounded growing, since it limits the normal plastic strain and the related compressive normal self-stress, as shown in Fig. 5b. The last modelled phenomenon is the strength reduction, which has been considered in order to reproduce the effect of smoothing asperities during the plastic sliding between the interface edges. The results obtained with the third model (EP with both dilatancy degradation and resistance reduction) are compared in figs. 6 with the results of the first model and of the second one, where a progressive reduction of the residual frictional tangential strength and a constant limited normal stress can be observed.

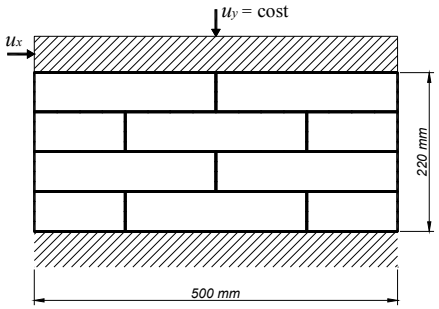

Figure 5: Structural scheme used for the numerical analysis**.**

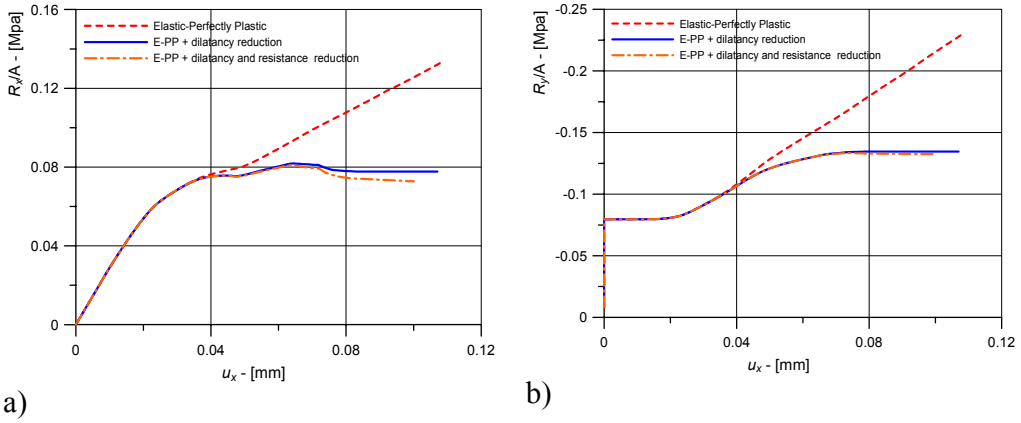

Figure 6: (a) Mean tangential and (b) mean normal stress at the top and at the bottom sections.

The same three models have been tested for a cyclic loading condition in which the same constant imposed vertical displacement at the top section ($u_y = -0.01$ mm) is applied plus a cyclic horizontal displacement history reported in Fig. 7. The effect of the dilatancy degradation, respect to the EPP model, are shown in Fig. 8a in terms of mean tangential stress at the constrained sections *vs* horizontal displacement; the EPP model exhibits an unlimited increasing strength whereas the dilatancy degradation limits the tangential strength and causes an higher hysteretic dissipation. The same effect of increasing normal load, observed for the monotonic load, is obtained for the cyclic test in Fig. 8b in terms of mean normal stress *vs* tangential displacement. Finally, the effect of the strength reduction and dilatancy degradation, in cyclic loading condition, is compared to the effect of only dilatancy degradation in Fig. 8b, where a decreasing residual strength can be observed cycle by cycle. Figure 9 shows that the mean normal

stress obtained by the proposed model remain constant after the dilatancy and strength saturationg branches.

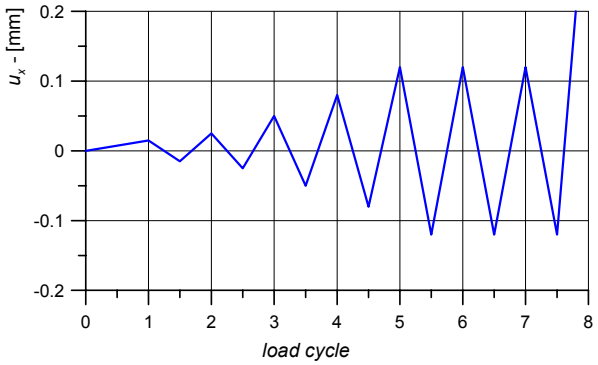

Figure 7: Cyclic loading low of the horizontal displacement.

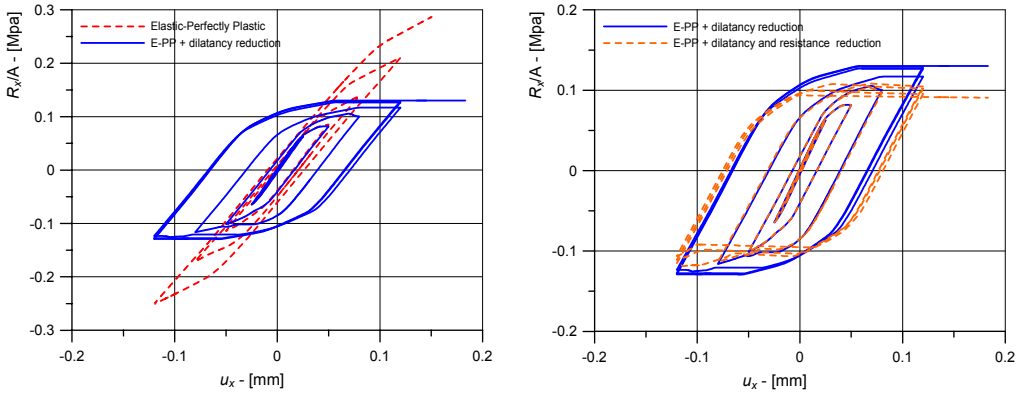

Figure 8: a) Mean tangential stress for the EPP model and in case of dilatancy degradation; b) Mean tangential stress for only dilatancy degradation and for dilatancy-strength degradation.

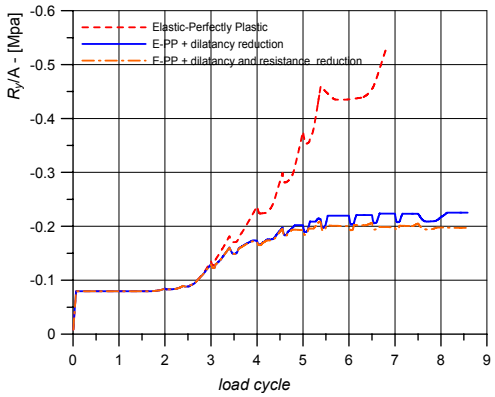

Figure 9: Mean normal stress at the top and at the bottom sections.

Acknowledgments: Financial support from the MIUR through Prin07 project 2007YZ3B24, *Multi-scale problems with complex interactions in Structural Engineering* is gratefully acknowledged.

References

[1] O. Allix, P. Ladeveze, Interlaminar interface modeling for the prediction of delamination, Int. J. Compos. Struct., 22 (4) (1992), 235-242.

[2] J.L. Chaboche, R. Girard, P. Levasseur, On the interface debonding models, Int. J. Damage Mech. 6, (1997) 220-257.

[3] J.L. Chaboche, R. Girard, A. Schaff, Numerical analysis of composite systems by using interphase/interface models, Comput Meth 20, (1997) 3-11.

[4] G. Alfano, M.A. Crisfield, Finite element interface models for the delamination analysis of laminated composites: mechanical and computational issues, I. Jour. Num. Meth. Eng. 50 (2001) 1701-1736.

[5] J.L. Chaboche, F. Feyel, Y. Monerie, Interface debonding models: a viscous regularization with a limited rate dependency Int. J. Solids Structures 38 (2001) 3127-3160.

[6] A. Caballero, K.J. Willam, I. Carol, Consistent tangent formulation for 3D interface modelling of cracking/fracture in quasi-brittle materials, Comput. Meth. Appl. Mech. Engrg. 197 (2008) 2804–2822

[7] I. Carol, C.M. Lopez, O. Roa, Micromechanical analysis of quasi-brittle materials using fracture-based interface elements. Int. J. Numer. Meth. Engng., 52 (2001) 193-215.

[8] N. Valoroso, L. Champaney, A damage-mechanics-based approach for modelling decohesion in adhesively bonded assemblies, Eng. Fract. Mech. 73 (2006) 2774–2801.

[9] G. Alfano, E. Sacco, Combining interface damage and friction in a cohesive-zone model, Int. J. Numer. Meth. Eng. 68 (2006) 542-582.

[10] G. Borino, A. Failla, F. Parrinello, A damage interface model with cohesive-frictiona continuous transition, M. Jirasek, Z. Bittnar, H. Mang (Eds.), Proc. ECCOMAS Thematic Conf. Modell. Heterog. Mater., Prague, Czech Republic, 2007 pag. 80-81.